



# Improved structural stability, electron transport and defect formation in $\text{PrBaCo}_{2-x}\text{Al}_x\text{O}_{6-\delta}$



S.N. Marshenya<sup>a</sup>, B.V. Politov<sup>a</sup>, A. Yu Suntsov<sup>a,\*</sup>, I.A. Leonidov<sup>a</sup>, S.A. Petrova<sup>b</sup>, M.V. Patrakeev<sup>a</sup>, V.L. Kozhevnikov<sup>a</sup>

<sup>a</sup> Institute of Solid State Chemistry UB RAS, 620990, Yekaterinburg, Russia

<sup>b</sup> Institute of Metallurgy UB RAS, 620016, Yekaterinburg, Russia

## ARTICLE INFO

### Article history:

Received 13 February 2018

Received in revised form

26 June 2018

Accepted 8 July 2018

Available online 12 July 2018

### Keywords:

Oxide materials

Electrical transport

Point defects

Thermal expansion

Vacancy formation

## ABSTRACT

The double perovskite-like solid solutions  $\text{PrBaCo}_{2-x}\text{Al}_x\text{O}_{6-\delta}$  are obtained via combustion of glycerol-nitrate organo-metallic precursors. The aluminum doping occurs favorable for mitigation of thermal expansion and stabilization of the tetragonal structure in a wide range of temperature changes. The variations of equilibrium oxygen content in  $\text{PrBaCo}_{1.9}\text{Al}_{0.1}\text{O}_{6-\delta}$  are measured with a coulometric titration technique, and analyzed in terms of defect chemistry. It is shown that aluminum incorporation is accompanied by formation of rigid  $\text{AlO}_6$  octahedra in the crystal structure and enhanced disproportionation of  $\text{Co}^{3+}$  cations. The developed defect model is successfully applied in order to explain the data for conductivity and thermopower. The structural stability, moderate thermal expansion and high conductivity represent an advantageous properties combination for the using of  $\text{PrBaCo}_{1.9}\text{Al}_{0.1}\text{O}_{6-\delta}$  cobaltite in various high-temperature solid state electrochemical devices.

© 2018 Elsevier B.V. All rights reserved.

## 1. Introduction

The layered double perovskite-like cobaltites  $\text{RBaCo}_2\text{O}_{6-\delta}$ , where R is a rare-earth metal, have attracted considerable interest as materials for the using as cathodes in intermediate temperature SOFCs [1,2], oxygen semi-permeable membranes [3,4], catalysts [5], oxygen sensors [6], etc. The potential of their application is related with the capability of the cobaltites to accommodate a large amount of oxygen vacancies favorable for fast oxygen transport and high level of electron conductivity provided by charge disproportionation of  $\text{Co}^{3+}$  cations. Still, such drawbacks as large thermal expansion coefficient (TEC) and insufficient stability toward reduction greatly impair the utility of the cobaltites. The efficient means of circumventing the noted deficiencies can be associated with the properties tuning via partial replacement of cobalt in the original crystalline lattice with other metals. For instance, the introduction of nickel and iron in place of cobalt is shown to favour a decrease of TEC values [7,8]. In this regard it should be noted additionally that a considerable part of the overall TEC in cobaltites occurs due to the oxygen depletion at heating [9]. Therefore, the

partial replacement of cobalt with metals having substantially stronger bonding with oxygen is expected to more expressly affect oxygen retention and structural robustness. Considering the necessity for the efficient dopants to be close in the size and charge to the regular cations for ensured substitution, we selected aluminum as a doping element in this work because of the excellent stability of the aluminum oxide at heating and low pressures of oxygen, i.e., very strong chemical bonds of aluminum with oxygen, and near equality of  $\text{Al}^{3+}$  and  $\text{Co}^{3+}$  ionic radii ( $r_{\text{Al}^{3+}}^{\text{VI}} = 0.535$  and  $r_{\text{Co}^{3+}}^{\text{VI}} = 0.545$ ) [10].

It is known that aluminum can readily replace B-site cations thus rendering considerable impact on functional properties of cubic perovskite-like oxides. For instance, Mori et al. observed improved structural stability and the TEC decrease of  $\text{La}_{0.9}\text{Sr}_{0.1}\text{CrO}_3$  at introduction of a small amount of aluminum in place of chromium [11]. Authors [12,13] also found that moderate aluminum substitution is favorable for mitigation of TEC in  $\text{SrFe}_{1-x}\text{Al}_x\text{O}_{3-\delta}$  and  $\text{La}_{0.5}\text{Sr}_{0.5}\text{Fe}_{1-x}\text{Al}_x\text{O}_{3-\delta}$ . At the same time, the effects of aluminum incorporation in the double perovskite-like cobaltites have not been considered yet. Therefore, the most conducting  $\text{PrBaCo}_2\text{O}_{6-\delta}$  cobaltite is selected as a parent oxide for aluminum doping in this work [14]. We studied aluminum solubility, structural features and defect equilibrium in the obtained solid solutions

\* Corresponding author.

E-mail address: [suntsov@ihim.uran.ru](mailto:suntsov@ihim.uran.ru) (A.Y. Suntsov).

$\text{PrBaCo}_{2-x}\text{Al}_x\text{O}_{6-\delta}$ . Special attention was given to the analysis of the temperature and oxygen pressure driven changes in thermal expansion, electrical conductivity and thermopower.

## 2. Experimental

In order to synthesize  $\text{PrBaCo}_{2-x}\text{Al}_x\text{O}_{6-\delta}$  we used high purity (99.99%) cobalt and aluminum powder metals, barium carbonate and praseodymium oxide  $\text{Pr}_6\text{O}_{11}$ . The starting materials were weighed in desirable proportions, placed in a quartz beaker and dissolved in nitric acid at 200 °C. Then glycerol was added in the solution in equimolar ratio to the sum of metal cations. The obtained mixture of organo-metallic complexes was subjected to evaporation at 200 °C till self-ignition of the residue occurred. The powder-like combustion product was carefully grinded and additionally fired at 900 °C to remove trace organics, pelletized at 2 kBar of uniaxial pressure, sintered at 1100–1200 °C for 20 h in the air, and cooled down to room temperature in the furnace.

X-ray powder diffraction (XRD) at room temperature was applied for phase purity control of the obtained materials with a Shimadzu XRD 7000 diffractometer (Cu-K $\alpha$  radiation). A D8 Advance diffractometer equipped with a high temperature HTK1200 N chamber was used for XRD measurements at heating from room temperature to 1000 °C. The XRD spectra were collected with the temperature step 5 °C and the acquisition time 545 s at each temperature. The processing of the diffraction data was carried out with the help of a DIFFRACplus: EVA calculation package [15] and ICDD PDF4 data base [16]. The unit cell parameters were calculated by making use of the least squares in a Celref calculation media [17].

The changes of oxygen content ( $6-\delta$ ) in as-prepared samples at heating in the air and reducing gas mixtures were determined with a Setaram Setsys Evolution – 18 thermoanalyzer. The treatment in 5%  $\text{H}_2$  – 95% Ar atmosphere at 900 °C resulted in the reduction of  $\text{PrBaCo}_{2-x}\text{Al}_x\text{O}_{6-\delta}$  to the mixture of  $\text{BaAl}_2\text{O}_4$ ,  $\text{Pr}_2\text{O}_3$  and BaO oxides, and cobalt metal. The respective mass decrease ( $\Delta m$ ) was used for calculations of oxygen content in the as-prepared samples. The expansion of the materials at heating in the air was measured by a Linseis L75 dilatometer with the using of dense  $3 \times 3 \times 10$  mm ceramic samples. The heating rate at the expansion measurements was 3 °C.

The changes of equilibrium oxygen content in the samples at variations of temperature ( $T$ ) and oxygen partial pressure  $p_{\text{O}_2}$  in the ambient gas phase were obtained by a coulometric titration technique in the isothermal mode of measurements with the temperature step of 50 °C. The titration cell was made of cubically stabilized zirconia oxygen solid electrolyte. Two pairs of platinum electrodes were deposited on the inner and outer sides of the cell, and served as an oxygen pump and a sensor. The wired measuring cell was placed in a similar larger cell where oxygen pressure was maintained nearly equal to the pressure inside the measuring cell. The using of such a ‘double-cell technique’ allowed us to achieve a high accuracy of oxygen content measurements with the uncertainty that did not exceed  $\Delta\delta = \pm 0.002$ . More experimental details can be found elsewhere [18]. The thermal analysis results obtained at heating in the air  $\log p_{\text{O}_2} = -0.678$  were used as reference for the coulometric titration data. The numerical computations were carried out in a Maple calculation media.

The rectangular ceramic samples  $2 \times 2 \times 15$  mm with the density near 98% of theoretical one were prepared for thermopower and four-probe d.c. conductivity measurements. The specimen for thermopower experimental determination was equipped with butt electrodes and thermocouples, and placed in the measuring cell along the external tubular heater which ensured the lengthwise

temperature gradient near 20 °C. Another wired specimen for conductivity measurements was set in a cross-wise orientation in order to ensure strict equality of temperature values at voltage probes. The measurements were carried out in an isothermal measuring mode at 700–950 °C with the temperature step 50 °C in the oxygen partial pressure range  $3 \cdot 10^{-6}$  – 0.7 atm. The oxygen pressure during the measurements was maintained and controlled with the help of a zirconia pump and a sensor, respectively. Additional experimental details can be found in work [19].

## 3. Results and discussion

XRD patterns in Fig. 1 for as-synthesized oxides  $\text{PrBaCo}_{2-x}\text{Al}_x\text{O}_{6-\delta}$ , where  $x = 0, 0.05, 0.10$  and  $0.15$ , give evidence to the aluminum solubility limit within  $0.1 < x < 0.15$  as precipitation of barium aluminate  $\text{BaAl}_2\text{O}_4$  [20] can be observed at  $x = 0.15$  while the sample  $x = 0.10$  is phase pure. The single phase aluminum doped materials crystallize with a tetragonal structure (S.G.  $P4/mmm$ ) in difference with the orthorhombic parent cobaltite  $\text{PrBaCo}_2\text{O}_{6-\delta}$  [21]. The tetragonal unit cell parameters  $a = b = 3.905$  and  $c = 7.633$  Å do not virtually depend on aluminum content, which is consistent with the replacement of  $\text{Co}^{3+}$  by  $\text{Al}^{3+}$  cations. The XRD pattern for the fully reduced sample  $\text{PrBaCo}_{1.9}\text{Al}_{0.1}\text{O}_{6-\delta}$  has been collected in the air, Fig. 2. The reduced material is seen to contain  $\text{Pr}(\text{OH})_3$  and  $\text{BaCO}_3$ . These forms are believed to appear in the result of the interaction of the primary reduction products  $\text{Pr}_2\text{O}_3$  and BaO, respectively, with water vapors and carbon dioxide in the air.

XRD data in Fig. 3 for  $\text{PrBaCo}_{1.9}\text{Al}_{0.1}\text{O}_{6-\delta}$  at temperature increase to 1000 °C show always tetragonal structure and the absence of phase admixtures, i.e. rather good structural stability of the aluminum doped derivative at heating in the air. The coincidence of crystal lattice parameters in the heating and cooling modes in Fig. 4 suggests thermal equilibration of the sample during the measurements. The small kinks near 300 °C on the plots in Fig. 4 reflect the incipient oxygen exchange between the sample and ambient gas phase. It should be stressed, however, that in difference with the

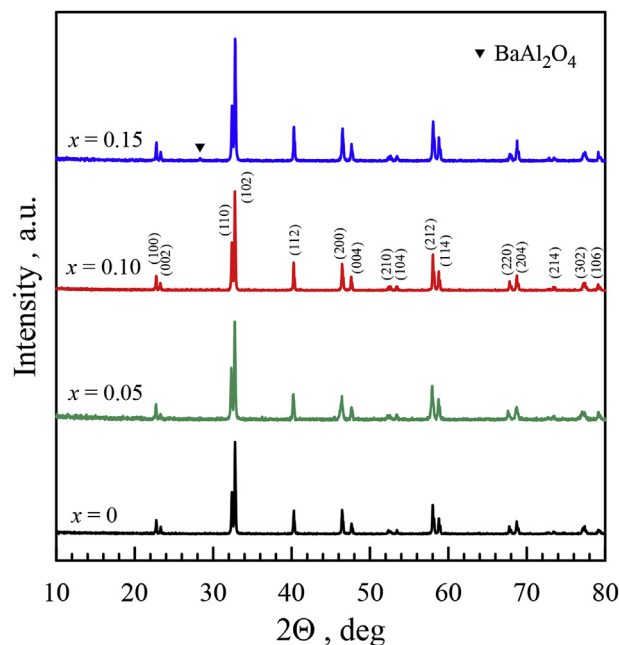


Fig. 1. The powder XRD spectra for  $\text{PrBaCo}_{2-x}\text{Al}_x\text{O}_{6-\delta}$ , where  $x = 0, 0.05, 0.10$  and  $0.15$ . The small peak near 28° is indicative of  $\text{BaAl}_2\text{O}_4$  phase admixture in the sample with  $x = 0.15$ .

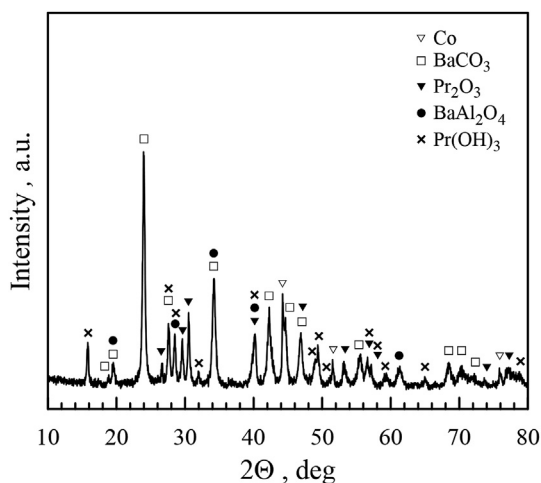


Fig. 2. XRD pattern for fully reduced  $\text{PrBaCo}_{1.9}\text{Al}_{0.1}\text{O}_{6-\delta}$  cobaltite.

parent cobaltite  $\text{PrBaCo}_2\text{O}_{6-\delta}$  where this singularity signals also a gradual transition from orthorhombic to tetragonal structure [21], the doped sample permanently retains the tetragonal structure.

The heating of the solid solution  $\text{PrBaCo}_{2-x}\text{Al}_x\text{O}_{6-\delta}$  results in oxygen depletion as it takes place in other double perovskite cobaltites [2,14]. The effect of aluminum doping is demonstrated in Fig. 5 where thermogravimetric data show that heating of the samples with larger aluminum content is accompanied with smaller weight loss. The oxygen content  $(6-\delta)=5.83$  in as-prepared sample  $x=0.1$  occurs larger compared to  $x=0$  as thermogravimetric reduction experiments reveal.

On the other hand, the substituted samples show decreased thermal expansion while the slopes of the relative elongation plots do not reveal any singular behaviour peculiar to  $\text{PrBaCo}_2\text{O}_{6-\delta}$ , Fig. 6. These results clearly show that replacement of cobalt for aluminum is beneficial for enhanced retention of oxygen in the crystalline structure, i.e., for the increase of the average metal – oxygen bonding energy in the cobaltites.

The experimental isothermal pressure dependent plots of oxygen content are shown in Fig. 7 for  $\text{PrBaCo}_{1.9}\text{Al}_{0.1}\text{O}_{6-\delta}$  as an example. In order to explain the observed changes in their shape we use the approach developed earlier [22–24]. With the cubic perovskite  $\text{PrCoO}_3$  as a reference crystal. We assume on the basis of the structural data that the aluminum substitution of quasi-neutral cobalt sites  $\text{Co}_{\text{Co}}^{\times}$  in  $\text{PrBaCo}_2\text{O}_{6-\delta}$  results in appearance of quasi-neutral defects  $\text{Al}_{\text{Co}}^{\times}$  in octahedral oxygen coordination that does not change with variations of  $T$  and  $p_{\text{O}_2}$ . As a result, oxygen positions around aluminum cations occur excluded from oxygen exchange in accord with the thermal analysis data that evidence

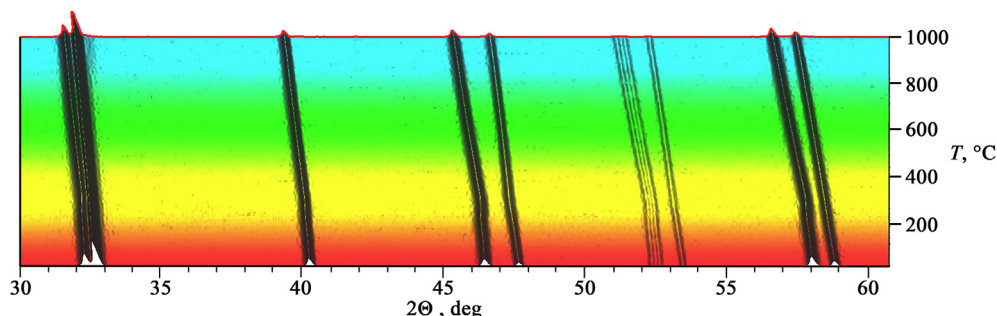


Fig. 3. The changes in positions of X-ray reflections for  $\text{PrBaCo}_{1.9}\text{Al}_{0.1}\text{O}_{6-\delta}$  at heating and cooling.

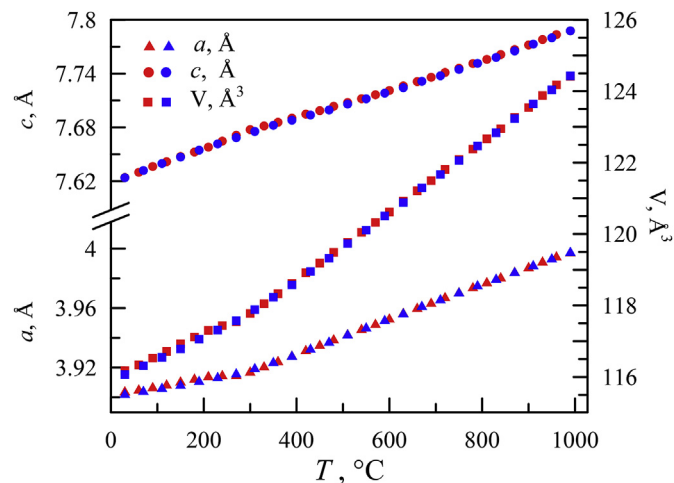


Fig. 4. The temperature dependent plots for the unit cell parameters in  $\text{PrBaCo}_{1.9}\text{Al}_{0.1}\text{O}_{6-\delta}$  at heating (red) and cooling (blue). (For interpretation of the references to colour in this figure legend, the reader is referred to the Web version of this article.)

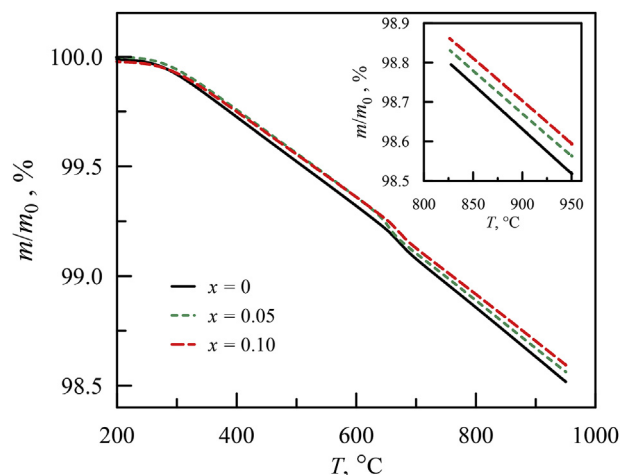


Fig. 5. The weight loss of  $\text{PrBaCo}_{2-x}\text{Al}_x\text{O}_{6-\delta}$  samples at heating in the air.

better retention of oxygen in the aluminium doped samples compared to the pristine cobaltite in heating.

It has been shown already [22–24] that defect equilibration in double-perovskite cobaltites takes place as a result of the simultaneous reactions

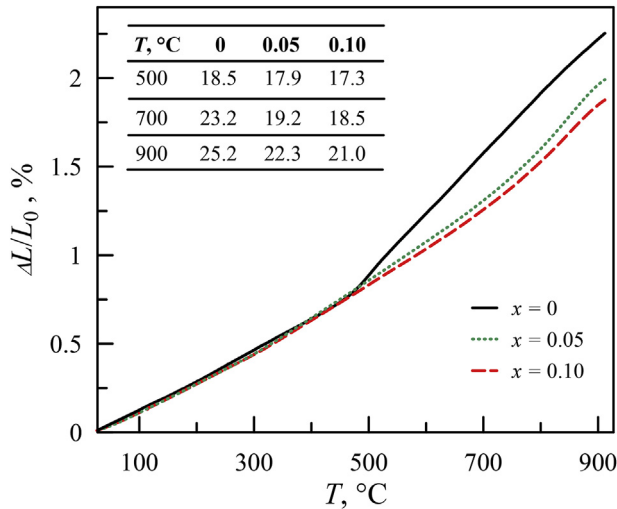


Fig. 6. The relative linear elongation of PrBaCo<sub>2-x</sub>Al<sub>x</sub>O<sub>6-δ</sub> samples at heating in the air. The average thermal expansion coefficient values ( $\cdot 10^6 \text{ K}^{-1}$ ) at selected temperatures are given in the inset table.

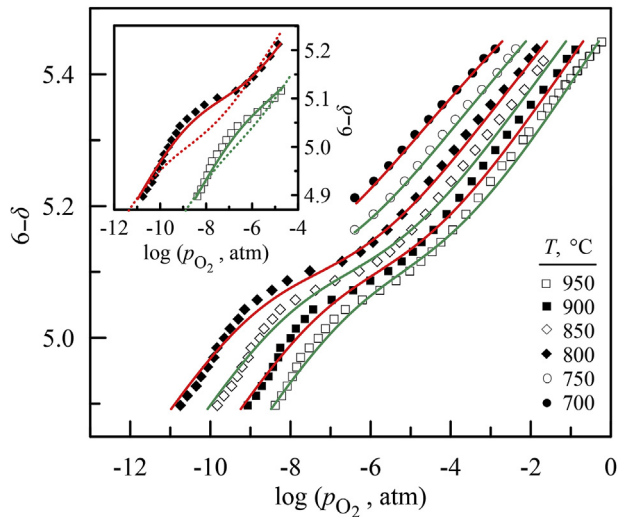


Fig. 7. The pressure dependent plots for oxygen content in PrBaCo<sub>1.9</sub>Al<sub>0.1</sub>O<sub>6-δ</sub> at different temperatures. Symbols represent experimental data; dotted and solid lines in the inset show results as calculated with the help of Eq. (20) at  $x=0$  and  $0.1$ , respectively.



where  $\text{V}_{\text{O}_2}^{\cdot\cdot}$ ,  $\text{V}_{\text{O}_3}^{\cdot\cdot}$ ,  $\text{O}_{\text{O}_2}^{\times}$ ,  $\text{O}_{\text{O}_3}^{\times}$ ,  $\text{Co}_{\text{Co}}^{\cdot}$  and  $\text{Co}_{\text{Co}}^{\times}$  designate vacant and filled O2 and O3 positions, and electron holes and electrons localized on cobalt atoms, respectively. As far as aluminum doping does not change electrical equilibrium in the crystalline lattice, the electrical neutrality condition for PrBaCo<sub>2-x</sub>Al<sub>x</sub>O<sub>6-δ</sub> remains the same as for PrBaCo<sub>2</sub>O<sub>6-δ</sub>

$$n = p + 2[\text{V}_{\text{O}_2}^{\cdot\cdot}] - 1 = p + 2\delta - 1 \quad (4)$$

while the structure conservation requirement must be presented as

$$g + p + n = 2 - [\text{Al}_{\text{Co}}^{\times}] = 2 - x \quad (5)$$

where  $[\text{Al}_{\text{Co}}^{\times}]$  stands for the concentration of Al<sub>Co</sub><sup>×</sup> defects, and symbols  $n$ ,  $p$  and  $g$  designate concentrations of localized electrons  $\text{Co}_{\text{Co}}^{\cdot}$ , holes  $\text{Co}_{\text{Co}}^{\times}$  and regular sites  $\text{Co}_{\text{Co}}^{\times}$ , respectively. The combination of the equilibrium constant for the intrinsic reaction (2)

$$K_{\text{cd}} = \frac{[\text{Co}_{\text{Co}}^{\cdot}] \cdot [\text{Co}_{\text{Co}}^{\times}]}{[\text{Co}_{\text{Co}}^{\times}]^2} = \frac{n \cdot p}{g^2} \quad (6)$$

with relations (4) and (5) results in the following expression

$$p = \frac{3}{2} - \delta - \frac{x}{2} + \frac{2 - x - \sqrt{D_{\text{cd}(0)} + D_{\text{cd}(x)}}}{2(4K_{\text{cd}} - 1)} \quad (7)$$

where

$$D_{\text{cd}(0)} = (2\delta - 1)^2 + 4K_{\text{cd}}(3 - 2\delta)(1 + 2\delta) - 16K_{\text{cd}} \quad (8)$$

$$D_{\text{cd}(x)} = -4K_{\text{cd}}(x - 2)^2 \quad (9)$$

It follows from (7) that the replacement of electroactive cobalt by aluminum cations is generally favorable for a decrease in the concentration of holes and, consequently, in the exclusion of the respective amount of holes from electric transport.

In order to calculate the oxygen vacancy concentrations in different crystallographic positions we have to use the equilibrium constant for reaction (3)

$$K_{\text{od}} = \frac{[\text{V}_{\text{O}_2}^{\cdot\cdot}] \cdot [\text{O}_{\text{O}_3}^{\times}]}{[\text{O}_{\text{O}_2}^{\times}] \cdot [\text{V}_{\text{O}_3}^{\cdot\cdot}]} \quad (10)$$

Additionally, we have to take into account oxygen positions supposedly excluded from gas exchange by aluminum. The respective amount can be easily calculated from binomial distribution under assumption of random spreading of aluminum dopants over the crystalline lattice of PrBaCo<sub>2-x</sub>Al<sub>x</sub>O<sub>6-δ</sub> as

$$[\text{O}_{\text{O}_i}^{\times}]_{(\text{excl})} = \sum_z \binom{2}{z} (x \cdot m_i)^z (1 - x \cdot m_i)^{2-z} \quad (11)$$

where  $z$  is the amount of aluminum ions near  $i$ 'th oxygen position, and  $m_i$  is the amount of oxygen ions in  $i$ 'th position per B-site in the elementary unit. Considering the crystalline lattice of the double-perovskite we can see that  $m_2 = 2$  and  $m_3 = 1/2$  for O2 and O3 positions, respectively. Therefore, the concentrations of O2 and O3 positions excluded from gas exchange follow as

$$[\text{O}_{\text{O}_2}^{\times}]_{(\text{excl})} = 4x(1 - x) \quad (12)$$

$$[\text{O}_{\text{O}_3}^{\times}]_{(\text{excl})} = \frac{x(4 - x)}{4} \quad (13)$$

while the concentrations of O2 and O3 positions available for gas exchange can be found from

$$[\text{O}_{\text{O}_2}^{\times}] = 4 - 4x(1 - x) - [\text{V}_{\text{O}_2}^{\cdot\cdot}] \quad (14)$$

$$[O_{O_3}^{\bullet}] = 1 - \frac{x(4-x)}{4} - [V_{O_3}^{\bullet}] \quad (15)$$

The total vacancy concentration is simply

$$[V_{O_2}^{\bullet}] + [V_{O_3}^{\bullet}] = \delta \quad (16)$$

The set of equations (10) and (14)–(16) can be used in order to find

$$[V_{O_2}^{\bullet}] + [V_{O_3}^{\bullet}] = \delta \quad (17)$$

where

$$D_{od(0)} = 16\{K_{od}^2(\delta - 4)^2 - 2K_{od}(\delta^2 - 5\delta - 4) + (\delta - 1)^2\} \quad (18)$$

$$D_{od(x)} = (16K_{od} + 1)x^3((16K_{od} + 1)(x - 4) - 4) + 8x(4K_{od} + 1) \times (3x - 4)(8K_{od} + 1) - 4 + 8x\delta(K_{od} - 1)((1 - x) \times (16K_{od} - 1) - 3) \quad (19)$$

Finally, the equilibrium pressure of oxygen over  $\text{PrBaCo}_{2-x}\text{Al}_x\text{O}_{6-\delta}$  follows from the equilibrium constants  $K_{Ox}$  and  $K_{cd}$  for reactions (1) and (2) as

$$p_{O_2} = \left( \frac{1}{K_{cd}K_{Ox}} \cdot \frac{[V_{O_3}^{\bullet}]}{[O_{O_3}^{\bullet}]} \cdot \frac{p}{n} \right)^2 \quad (20)$$

where variables (4), (7), (15) and (17) are to be used. The calculated values of the pressure may change with temperature because of the equilibrium constants  $K_{Ox}$  and  $K_{cd}$  that depend on temperature as

$$K_j = \exp\left(\frac{\Delta S_j^\circ}{R}\right) \cdot \exp\left(\frac{-\Delta H_j^\circ}{R(T + 273)}\right) \quad (21)$$

where  $\Delta H_j^\circ$  and  $\Delta S_j^\circ$  denote changes in standard enthalpy and entropy for the respective  $j$ 'th defect formation reaction  $R$  is the gas constant. Respectively, the independent variations of enthalpies  $\Delta H_j^\circ$  and entropies  $\Delta S_j^\circ$  for reactions (1), (2) and (3) are to be employed in order to simulate the experimental results for  $\log p_{O_2} = f(T, \delta, x)$  in Fig. 7. It is distinctly seen in the figure inset that the disregard of the exclusion effects by setting  $x = 0$  does not allow obtaining satisfactory fitting, particularly in the low-pressure range. The calculated thermodynamic parameters for reactions (1), (2), and (3) in  $\text{PrBaCo}_{1.9}\text{Al}_{0.1}\text{O}_{6-\delta}$  are shown in Table 1 together with the respective values in  $\text{PrBaCo}_{1.8}\text{Ni}_{0.2}\text{O}_{6-\delta}$  [23] and  $\text{PrBaCo}_2\text{O}_{6-\delta}$  [24] for comparison. It can be seen that the standard enthalpy and entropy changes for defect formation reactions are virtually independent on the content of either  $\text{Ni}^{2+}$  or  $\text{Al}^{3+}$ . Consequently, the free energy  $\Delta G_{\text{Red}}^\circ$  for reduction of  $\text{Co}^{3+}$  to  $\text{Co}^{2+}$  in

**Table 1**  
The standard entropy and enthalpy values for defect formation reactions (1)–(3).

Reaction	$\Delta S_j^\circ$ , J/mol·K			$\Delta H_j^\circ$ , kJ/mol		
	(1)	(2)	(3)	(1)	(2)	(3)
$\text{PrBaCo}_{1.9}\text{Al}_{0.1}\text{O}_{6-\delta}$	$-100 \pm 5$	$15 \pm 9$	$-20 \pm 6$	$-152 \pm 5$	$53 \pm 10$	$61 \pm 7$
$\text{PrBaCo}_{1.8}\text{Ni}_{0.2}\text{O}_{6-\delta}$	$-103 \pm 4$	$21 \pm 4$	$-20 \pm 3$	$-152 \pm 5$	$59 \pm 3$	$63 \pm 5$
$\text{PrBaCo}_2\text{O}_{6-\delta}$	$-60 \pm 5$	$-13 \pm 2$	$-40 \pm 4$	$-116 \pm 7$	$31 \pm 3$	$127 \pm 8$

$\text{PrBaCo}_{1.9}\text{Al}_{0.1}\text{O}_{6-\delta}$ , which may serve as a measure of phase stability at low pressures of oxygen [23], must be about the same as in  $\text{PrBaCo}_{1.8}\text{Ni}_{0.2}\text{O}_{6-\delta}$  so that the both derivatives should exhibit the same capability to withstand reducing atmospheres. One can notice also that nickel occurs about twice less efficient a dopant for enhanced structural robustness of the cobaltite than aluminum. This observation is in accord with stronger aluminum – oxygen bonding.

The plots in Fig. 8 show variations of electrical conductivity in  $\text{PrBaCo}_{2-x}\text{Al}_x\text{O}_{6-\delta}$ , where  $x = 0$  and 0.1, with temperature and equilibrium pressure of oxygen in the gas phase. It is seen rather unexpectedly that incorporation of electrically inactive aluminum in the structure is accompanied with some increase of the conductivity. In order to understand such a behaviour it is instructive to consider changes in the concentration of holes related to the unit cell volume  $V_{\text{cell}}^T$ .

$$C_h = \frac{N \cdot [Co_{Co}^{\bullet}]}{V_{\text{cell}}^T \cdot ([Co_{Co}^{\bullet}] + [Co_{Co}^{\times}] + [Co_{Co}^{\bullet}])} \quad (22)$$

where  $N = 2$  is the number of formula units in the referred perovskite  $\text{Pr}_{0.5}\text{Ba}_{0.5}\text{CoO}_{3-\delta/2}$ . The oxygen partial pressure and temperature driven variations in concentrations of electron defects and regular sites can be calculated from (4), (5) and (7) while changes of the unit cell with temperature are shown in Fig. 4. The respectively calculated data demonstrate that the concentration of holes at oxygen pressure variations in isothermal conditions appears to be larger in the aluminum doped sample as it may be deduced from the conductivity in Fig. 8. At the same time, the thermopower measurements unambiguously show  $p$ -type dominating charge carriers, Fig. 9. Considering that the high-temperature thermopower  $S$  for localized positive charge carriers is proportional to  $\log(1/C_h)$  [25], we find that the increasing thermopower signals the hole concentration decreasing with pressure in apparent agreement with the conductivity data.

Nevertheless, the pressure dependent plots in Figs. 8 and 9 are insufficient to unambiguously interpret the apparent increase of conductivity. Let's consider the electrical conductivity in the system of localized charge carriers. In the thermodynamic treatment above

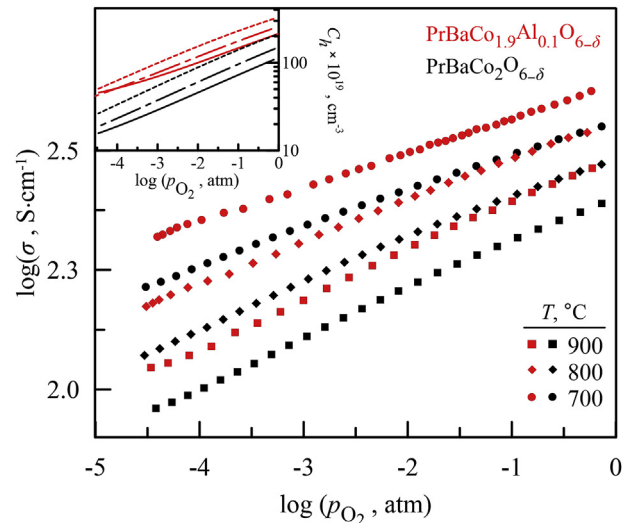


**Fig. 8.** The data for equilibrium isothermal total conductivity in  $\text{PrBaCo}_{2-x}\text{Al}_x\text{O}_{6-\delta}$ , where  $x = 0$  and 0.1, at variations of oxygen partial pressure. The variations in concentrations of electron holes are shown in the inset as calculated with the help of Eq. (22) at 700°C (dotted lines), 800°C (dashed lines) and 900°C (solid lines).

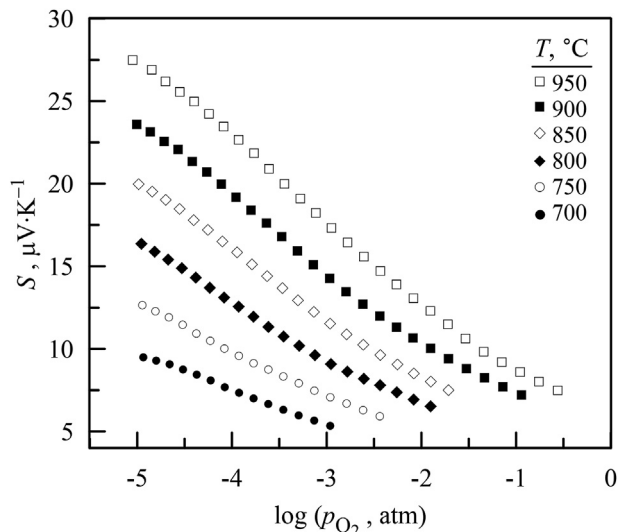


Fig. 9. Isothermal dependencies of thermopower in  $\text{PrBaCo}_{1.9}\text{Al}_{0.1}\text{O}_{6-\delta}$  vs  $\log(p_{\text{O}_2})$ .

it is proportional to the product of the charge carrier concentration  $p \equiv [\text{Co}^{4+}]$  by the number of positions  $[\text{Co}^{3+}]$  available for their jumps, i.e.,  $\sigma(T, \delta, x) \sim [\text{Co}^{3+}] \cdot [\text{Co}^{4+}]$ . Hence, interrelations (4), (5) and (7) can be used for the calculations. The respective results are shown in Fig. 10a where changes in concentrations of different cobalt species are shown at variations of oxygen content. One can observe that introduction of aluminum is accompanied with some increase in the concentration of electron holes. At the same time, the decrease in the concentration of available positions is more considerable so that the product  $[\text{Co}^{3+}] \cdot [\text{Co}^{4+}]$  and the conductivity  $\sigma(T, \delta, x)$  both tend to decrease with the increase of aluminum content at least at  $\delta$ 's within  $(6 - \delta) < 5.5$ . In order to compare the calculation results with the experiment we have to combine the electrical conductivity in Fig. 8 with the equilibrium oxygen content data in Fig. 7 so that to find variations of conductivity with oxygen content as shown in Fig. 10b. It is clearly seen that oxygen non-stoichiometry most strongly affects the conductivity, while temperature variations at permanent oxygen content are so small that different isotherms in Fig. 10b practically merge on the figure scale. Moreover, when considered at equal oxygen content, aluminum doping indeed, as expected, results in a decline of conductivity, which is confirmed with the calculated concentration of electron defects in Fig. 10a.

#### 4. Conclusions

The solid solutions  $\text{PrBaCo}_{2-x}\text{Al}_x\text{O}_{6-\delta}$ , where  $x = 0, 0.05, 0.10$  and  $0.15$ , are obtained via combustion of glycerol-nitrate precursors. The aluminum solubility limit is found to be within  $0.10 < x < 0.15$ . The single phase specimen  $x = 0.10$  is shown to maintain invariably tetragonal structure at heating in the air from room temperature to  $1000^\circ\text{C}$ . It is argued that the aluminum incorporation is accompanied with enhanced retention of oxygen in the structure at heating, and appreciable decrease of the thermal expansion coefficient. The analysis of defect equilibrium reactions is consistent with the supposition of aluminum dopants maintaining rigid octahedral oxygen coordination at any variations of temperature and oxygen partial pressure. The electron conductivity level in the doped samples occurs higher than in the pristine cobaltite in similar isobaric conditions due to larger oxygen content and, consequently, larger concentration of electron holes. The high conductivity level, moderate thermal expansion and structural stability are favorable

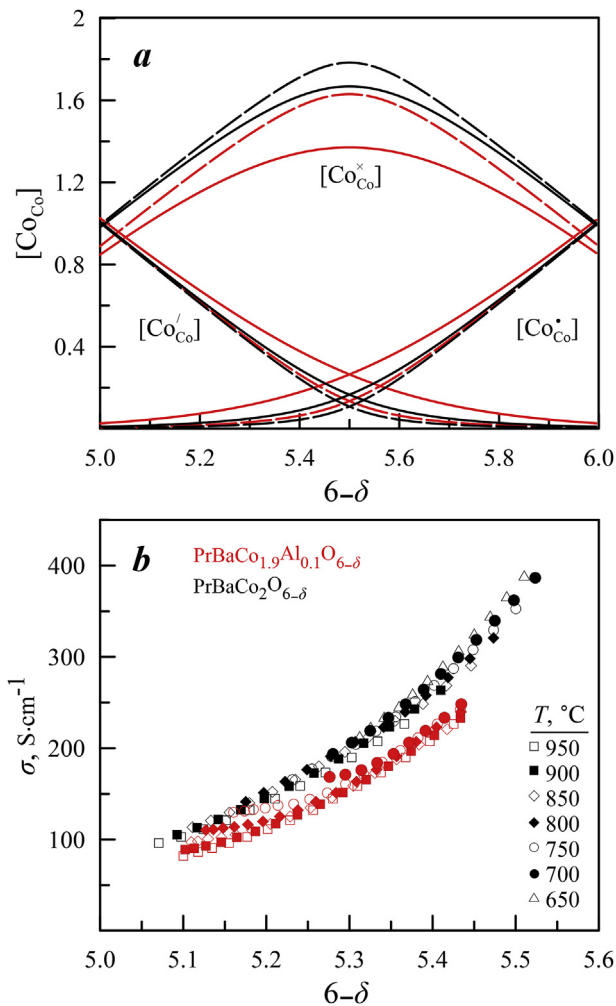


Fig. 10. The calculated oxygen content dependent changes in concentrations of different cobalt species (a) and measured total conductivity (b) in  $\text{PrBaCo}_{2-x}\text{Al}_x\text{O}_{6-\delta}$ , where  $x=0$  and  $0.1$ . The dashed and solid lines show results at  $700$  and  $950^\circ\text{C}$ , respectively. The experimental data for  $x=0$  are taken from Ref. [24].

features for the using of  $\text{PrBaCo}_{1.9}\text{Al}_{0.1}\text{O}_{6-\delta}$  in electrochemical devices designed to work at elevated temperatures.

#### Acknowledgements

This work is supported by the Russian Foundation for Basic Research under grant N<sup>o</sup>16–33–60202.

#### References

- [1] C. Sun, R. Hui, J. Roller, Cathode materials for solid oxide fuel cells: a review, *J. Solid State Electrochem.* 14 (2010) 1125–1144.
- [2] R. Pelosato, G. Cordaro, D. Strucchi, C. Cristiani, G. Dotelli, Cobalt based layered perovskites as cathode material for intermediate temperature Solid Oxide Fuel Cells: a brief review, *J. Power Sources* 298 (2015) 46–67.
- [3] A. Chronos, B. Yildiz, A. Tarancon, D. Parfitt, J.A. Kilner, Oxygen diffusion in solid oxide fuel cell cathode and electrolyte materials: mechanistic insights from atomistic simulations, *Energy Environ. Sci.* 4 (2011) 2774–2789.
- [4] T. Chen, H. Zhao, Z. Xie, N. Xu, Y. Lu, Oxygen permeability of  $\text{Ce}_{0.8}\text{Sm}_{0.2}\text{O}_{2-\delta}$ - $\text{LnBaCo}_2\text{O}_{5+\delta}$  ( $\text{Ln}=\text{La, Nd, Sm, and Y}$ ) dual-phase ceramic membranes, *Ionics* 21 (2015) 1683–1692.
- [5] A. Grimaud, K.J. May, C.E. Carlton, Y.L. Lee, M. Risch, W.T. Hong, J. Zhou, Y. Shao-Hong, Double perovskites as a family of highly active catalysts for oxygen evolution in alkaline solution, *Nat. Commun.* 4 (2013) 2439.
- [6] H. Song, Z. Qin, F. Gao, J. Jia, D. Yang, X. Hu, High temperature oxygen sensing properties of oxygen deficient  $\text{RBaCo}_2\text{O}_{5+\delta}$  thick films, *Sensor. Actuator. B Chem.* 177 (2013) 50–54.

- [7] J.-H. Kim, A. Manthiram, Layered  $\text{NdBaCo}_{2-x}\text{Ni}_x\text{O}_{5+\delta}$  perovskite oxides as cathodes for intermediate temperature solid oxide fuel cells, *Electrochim. Acta* 54 (2009) 7551–7557.
- [8] V.A. Cherepanov, T.V. Aksenova, L.Y. Gavrilova, K.N. Mikhaleva, Structure, nonstoichiometry and thermal expansion of the  $\text{NdBa}(\text{Co,Fe})_2\text{O}_{5+\delta}$  layered perovskite, *Solid State Ionics* 188 (2011) 53–57.
- [9] B. Wei, Z. Lü, D. Jia, X. Huang, Y. Zhang, W. Su, Thermal expansion and electrochemical properties of Ni-doped  $\text{GdBaCo}_2\text{O}_{5+\delta}$  double-perovskite type oxides, *Int. J. Hydrogen Energy* 35 (2010) 3775–3782.
- [10] R.D. Shannon, Revised effective ionic radii and systematic studies of interatomic distances in halides and chalcogenides, *Acta Crystallogr. A* 32 (1976) 751–767.
- [11] M. Mori, Y. Hiei, T. Yamamoto, Control of the thermal expansion of strontium-doped lanthanum chromite perovskites by B-site doping for high-temperature solid oxide fuel cell separators, *J. Am. Ceram. Soc.* 84 (2001) 781–786.
- [12] A.L. Shaula, V.V. Kharton, N.P. Vyshatko, E.V. Tsipis, M.V. Patrakeev, F.M.B. Marques, J.R. Frade, Oxygen ionic transport in  $\text{SrFe}_{1-y}\text{Al}_y\text{O}_{3-\delta}$  and  $\text{Sr}_{1-x}\text{Ca}_x\text{Fe}_{0.5}\text{Al}_{0.5}\text{O}_{3-\delta}$  ceramics, *J. Eur. Ceram. Soc.* 25 (2005) 489–499.
- [13] A.A. Yaremchenko, M.V. Patrakeev, V.V. Kharton, F.M.B. Marques, I.A. Leonidov, V.L. Kozhevnikov, Oxygen ionic and electronic conductivity of  $\text{La}_{0.3}\text{Sr}_{0.7}\text{Fe}(\text{Al})\text{O}_{3-\delta}$  perovskites, *Solid State Sci.* 6 (2004) 357–366.
- [14] J.H. Kim, A. Manthiram, Layered  $\text{LnBaCo}_2\text{O}_{5+\delta}$  perovskite cathodes for solid oxide fuel cells: an overview and perspective, *J. Mater. Chem. A* 3 (2015), 24195–24120.
- [15] DIFFRAC<sup>Plus</sup>; EvaBruker AXS GmbH, Ostliche Rheinbrückenstraße, vol. 50, 2008. D-76187, Karlsruhe, Germany.
- [16] Powder Diffraction File PDF4+ ICDD Release, 2016.
- [17] J. Laugier, B. Bochu, Lmgp-suite of programs for the interpretation of x-ray experiments. ENSP, Grenoble Lab. Matériaux Genie Phys. (2003).
- [18] M.V. Patrakeev, I.A. Leonidov, V.L. Kozhevnikov, Applications of coulometric titration for studies of oxygen non-stoichiometry in oxides, *J. Solid State Electrochem.* 15 (2011) 931–954.
- [19] M.V. Patrakeev, E.B. Mitberg, A.A. Lakhtin, I.A. Leonidov, V.L. Kozhevnikov, V.V. Kharton, M. Avdeev, F.M.B. Marques, Oxygen nonstoichiometry, conductivity, and seebeck coefficient of  $\text{La}_{0.3}\text{Sr}_{0.7}\text{Fe}_{1-x}\text{Ga}_x\text{O}_{2.65+\delta}$  perovskites, *J. Solid State Chem.* 167 (2002) 203–213.
- [20] A.J. Perrotta, J.V. Smith, *Bulletin Society Fr. Mineral Crystallography*, vol. 91, 1968, p. 85.
- [21] S. Streule, A. Podlesnyak, D. Sheptyakov, E. Pomjakushina, M. Stingaciu, K. Conder, M. Medarde, M.V. Patrakeev, I.A. Leonidov, V.L. Kozhevnikov, High-temperature order-disorder transition and polaronic conductivity in  $\text{PrBaCo}_2\text{O}_{5.48}$ , *Phys. Rev. B* 73 (2006), 094203.
- [22] A.Yu. Suntsov, B.V. Politov, I.A. Leonidov, M.V. Patrakeev, V.L. Kozhevnikov, Improved stability and defect structure of yttrium doped cobaltite  $\text{PrBaCo}_2\text{O}_{6-\delta}$ , *Solid State Ionics* 295 (2016) 90–95.
- [23] B.V. Politov, A.Yu. Suntsov, I.A. Leonidov, M.V. Patrakeev, V.L. Kozhevnikov, High-temperature defect thermodynamics of nickel substituted double-perovskite cobaltite  $\text{PrBaCo}_{2-x}\text{Ni}_x\text{O}_{6-\delta}$  ( $x = 0.2$ ), *J. Alloys Compd.* 727 (2017) 778–784.
- [24] A.Yu. Suntsov, I.A. Leonidov, M.V. Patrakeev, V.L. Kozhevnikov, Defect formation in double perovskites  $\text{PrBaCo}_{2-x}\text{Cu}_x\text{O}_{5+\delta}$  at elevated temperatures, *Solid State Ionics* 274 (2015) 17–23.
- [25] A.G. Bosman, H.J. van Daal, Small-polaron versus band conduction in some transition-metal oxides, *Adv. Phys.* 19 (1970) 1–117.